Journal of Hazardous Materials 163 (2009) 1040–1051

Contents lists available at ScienceDirect

Journal of Hazardous Materials

journal homepage: www.elsevier.com/locate/jhazmat

The simulation of air recirculation and fire/explosion phenomena within a semiconductor factory

Yet-Pole I*, Yi-Long Chiu, Shi-Jen Wu

Department of Safety, Health, and Environmental Engineering, National Yunlin University of Science and Technology, Touliu 640, Taiwan

ARTICLE INFO

Article history:
Received 1 February 2008
Received in revised form 6 June 2008
Accepted 14 July 2008
Available online 3 August 2008

Keywords:
Consequence analysis
Semiconductor
Air recirculation
Deflagration
Computational fluid dynamics

ABSTRACT

The semiconductor industry is the collection of capital-intensive firms that employ a variety of hazardous chemicals and engage in the design and fabrication of semiconductor devices. Owing to its processing characteristics, the fully confined structure of the fabrication area (fab) and the vertical airflow ventilation design restrict the applications of traditional consequence analysis techniques that are commonly used in other industries. The adverse situation also limits the advancement of a fire/explosion prevention design for the industry. In this research, a realistic model of a semiconductor factory with a fab, sub-fabrication area, supply air plenum, and return air plenum structures was constructed and the computational fluid dynamics algorithm was employed to simulate the possible fire/explosion range and its severity. The semiconductor factory has fan module units with high efficiency particulate air filters that can keep the airflow uniform within the cleanroom. This condition was modeled by 25 fans, three layers of porous ceiling, and one layer of porous floor. The obtained results predicted very well the real airflow pattern in the semiconductor factory. Different released gases, leak locations, and leak rates were applied to investigate their influence on the hazard range and severity. Common mitigation measures such as a water spray system and a pressure relief panel were also provided to study their potential effectiveness to relieve thermal radiation and overpressure hazards within a fab. The semiconductor industry can use this simulation procedure as a reference on how to implement a consequence analysis for a flammable gas release accident within an air recirculation cleanroom.

1. Introduction

The semiconductor industry is not only a capital and technological intensive industry but also a high-risk industry. Owing to the diversity of hazardous materials such as silane, phosphine, hydrogen, isopropyl alcohol, dichlorosilane, and the like that are often used during different processing operations, a fire and explosion accident might happen if any one of these materials were released from a leaking pipe, storage tank, or machinery [1], not to mention that some of them can even be poisonous to people and the environment. A fire and explosion accident cannot only cause human casualty and property damage, but the smoke particles arising from an incomplete combustion can also threaten the cleanliness of the fabrication area (fab) and severely damage the quality of the products. Therefore, how to prevent fire and explosion accidents and secure the integrity of a semiconductor plant has become a major issue for the industry. Owing to the characteristics of a totally confined fab structure and its air recirculation behavior, some semi-empirical consequence analysis models such as SAFETI or ALOHA and the like that have been commonly used in the petrochemical industry cannot be employed in the simulation of a semiconductor factory.

Nowadays with the great improvement of the computational ability in computers, the computational fluid dynamics (CFD) technique has become more and more advanced during recent years and has been utilized in different areas such as mechanical, chemical, civil, and safety engineering [2–6]. It is believed that a properly designed CFD model cannot only simulate possible fire and explosion scenarios in a cleanroom (C/R) but also can test different hazard mitigation measures at the same time. However, how to simulate an air recirculation pattern in a fab building and simultaneously maintain a laminar airflow within the C/R region has become a great challenge to researchers [7].

In this study, various airflow mechanisms are designed and simulated. It is found that certain equally spaced fans blowing through three porous layers can vividly simulate the function of the fan module unit (FMU) layer and produce realistic airflow patterns. Different simulation scenarios such as released gas categories, leak locations, leak rates, drop diameters of the water spray, and

* Corresponding author. Tel.: +886 5 5342601x4421/4493/4496; fax: +886 5 5312069.
E-mail addresses: iyp@yuntech.edu.tw, iyetpole@es.yuntech.edu.tw (Y.-P. I).

0304-3894/$ – see front matter © 2008 Published by Elsevier B.V.
doi:10.1016/j.jhazmat.2008.07.117

Nomenclature

CL	cleanliness level
CFD	computational fluid dynamics
CMP	chemical-mechanical planarization or chemical-mechanical polishing
CASD	computer-aided scenario design, a preprocessing module of FLACS
C/R	cleanroom
DDT	deflagration to detonation
D_m	mean droplet diameter or Sauter diameter (μm)
fab	fabrication area
EMO	emergency shutoff
F	an airflow modelling design which is composed of 25 fans
F+L	an airflow modelling design which is composed of 25 fans with three layers of porous ceiling
FFUs	fan filter units
FLACS	flame acceleration simulator, a kind of CFD software
Flacs	a core calculating module of FLACS
Flowvis	flow visualization, a post-processing module of FLACS
FMUs	fan module units
HEPA	high efficiency particulate air (filter)
I	the variable of grid number at *X*-axis
J	the variable of grid number at *Y*-axis
K	the variable of grid number at *Z*-axis
L	an airflow modelling design which is composed of three layers of porous ceiling
N	an airflow modelling design which is composed of 36 nozzles with one fan (located at RAP area)
P	a mitigation measure, which contains a pressure relief panel only
(Po_i, Po_f)	initial and final degree of porosity for the pressure relief panel
P_w	water pressure (Pa) (see Table 2)
Q	water flow-rate ($m^3\ s^{-1}$) (see Table 2)
Q_m	leak rate of hazardous material ($kg\ s^{-1}$) (see Table 1)
RAP	return air plenum
S	a mitigation measure which contains a water spray system only
S+P	a mitigation measure which contains both a water spray system and a pressure relief panel
SAP	supply air plenum
subfab	sub-fabrication area
U_z	average droplet velocity vertically downward (absolute value) ($m\ s^{-1}$) (see Table 2)
ULPA	ultra-low penetration air (filter)
VVEC	airflow velocity vector ($m\ s^{-1}$) (see Fig. 5)
W	airflow velocity component at *Z*-axis ($m\ s^{-1}$) (see Fig. 5)
X_{HI}	boundary plane at *X*-axis (with the highest coordinate value)
X_{LO}	boundary plane at *X*-axis (with the lowest coordinate value)
(*x*, *y*, *z*)	Cartesian coordinate
Y_{HI}	boundary plane at *Y*-axis (with the highest coordinate value)
Y_{LO}	boundary plane at *Y*-axis (with the lowest coordinate value)
Z_{HI}	boundary plane at *Z*-axis (with the highest coordinate value)
Z_{LO}	boundary plane at *Z*-axis (with the lowest coordinate value)

Greek letter

β_{water}	volume fraction of water (‰) (see Table 2)

mitigation facilities are also discussed. The simulation results can be demonstrated in a 3D dynamic format to related personnel. These results not only can facilitate the understanding of different hazard evolutions but also can be provided as the safety design references for a semiconductor factory.

2. Structure and function of a semiconductor factory

The current layout of a modern semiconductor factory usually contains four parts (see Fig. 1), that is (1) supply air plenum (SAP), which includes fan chamber and filter chamber; (2) C/R or fab, which includes process areas, work areas, preparation areas (divided according to different "class numbers" or "cleanliness levels (CL)," as the process requires), and a free access zone; (3) subfabrication area (subfab) or utility space; and (4) return air plenum (RAP) or central return air space. The SAP is usually located at the top of a fab and mainly provides clean airflow that a C/R needs. Different air supply equipment such as the fan filter units (FFUs), FMUs with filters, and so forth have been designed for this purpose. The fab area is the common name for a place where wafers go through a series of lithography, etching, thin film, diffusion, and chemical-mechanical planarization (CMP) processes that need an extra-clean air environment. A subfab is usually located below a C/R and contains many pipes and equipment for material supplies (such as process gases, chemicals, and pure water) and exhaust treatment. The RAP area is a vertical space within the factory building to form an air recirculation duct, which usually includes a set of humidity controlled/temperature conditioning facilities located near the subfab. The down-flowing air from the C/R first passes through the airflow guide pits below the perforated raised-floor, then flows through the central return-air space, and returns to the supply chamber again.

A semiconductor C/R [9] has a very complicated structure and its major mission is for chip production. All the wafer manufacturing processes are finished in this area. Its cleanliness levels are differentiated according to the processing requirements (usually varies from CL1 to CL1000 in a 200 mm wafer manufacturing fab). This clean air environment is mainly maintained by the FMUs, filters, and perforated raised-floors. The FMUs, located above the filter chamber of a C/R, are a series of very large fan modules for supplying airflow. Below them, different filter structures such as the high efficiency particulate air (HEPA) or ultra low penetration air (ULPA) filters are designed to eliminate dust within the recirculated air, produce laminar airflow to the C/R, and maintain the cleanliness levels of different C/R chambers. The raised-floor with perforated panels is supported by the structure rods above the airflow guide pits. The downward laminar air flowing through the perforated floor can sweep out most of the dust produced by personnel and operations in a C/R.

3. Research methods

3.1. Software introduction

A fire and explosion CFD software called FLACS (Flame Acceleration Simulator) was employed in this study. FLACS was designed

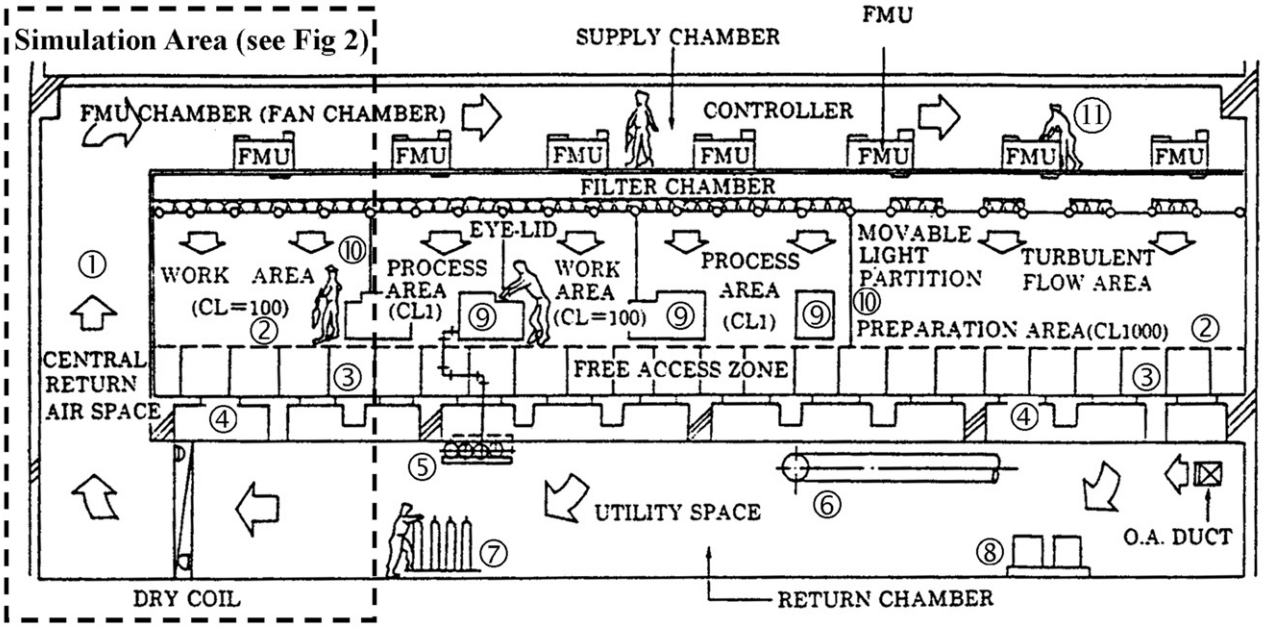

Fig. 1. Cross-sectional diagram of a semiconductor factory [8], where the numbers denote: (1) airflow direction, (2) raised-floor or porous floor, (3) floor support, (4) guide pit/hole, (5) chemical supply lines, (6) gases exhaust duct, (7) gas bottles, (8) pumps, (9) manufacturing machinery and (10) separation wall, operator with bunny suit.

to simulate the consequences of a flammable gas release within a semi-confined space or an open site area [10]. With its 3D dynamic characteristics, the FLACS simulation results can be observed from any angle, distance, or different cross-sectional planes, thus facilitating the understanding of the spatial and temporal distribution of many "physical variables in the fluid field" (such as overpressure, impulse pressure, temperature, ventilation velocity, and so on) that cannot be observed by traditional simulation software. FLACS is composed of three parts as follows:

(1) Computer-aided scenario design (CASD)

This is a preprocessing module that can build 3D models to simulate different terrains and building structures, define different sizes and numbers of grids to divide up the model-excluded space, set up boundary conditions and many other parameters used for simulation.

(2) Flacs numerical calculating module

This module is the core program of the software. Its calculation algorithms include conservation equations for mass, momentum, enthalpy, mass fraction of chemical species, turbulent kinetic energy, and dissipation rate of turbulent kinetic energy. All these six sets of governing equations can be found in the books of compressible flow theory [11,12]. FLACS uses the SIMPLE method and other submodels to implement a 3D numerical simulation [13]. Lots of explosion experiments conducted for developing and

Table 1
List of different simulation scenarios and their corresponding parameters

Scenario code	1A	1B	1C	2A[a]	2B	3A[a]	3B	4A[a]	4B	5A	5B	5C[b]	6A[b]	6B	6C
Airflow modeling[c]	N	F	F+L	F+L		F+L		F+L		F+L			F+L		
Gas category	N/A[d]			C_3H_8	H_2	C_3H_8		C_3H_8		C	$_3H_8$		C_3H_8		
Leak location[e]	N/A			subfab		subfab	C/R	subfab		subfab			subfab		
Leak rate, Q_m (kg s^{-1})	N/A			0.2		0.2		0.2	0.4	0.2			0.2		
Mean droplet diameter of water spray, D_m (μm)	N/A			N/A		N/A		N/A		700	1000	846	846	N/A	846
Mitigation measures[f]	N/A			N/A		N/A		N/A		S			S	P	S+P

[a]Scenarios 2A, 3A, 4A are all the same; they are employed as the "basis scenario of fire/explosion" for comparison purpose; [b]Scenarios 5C and 6A are equal; they are employed as the "basis scenario of fire/explosion with water mitigation" for comparison purpose; [c]N: 36 nozzles with one fan located at RAP area; F: 25 fans; L: three layers of porous ceiling; F+L: 25 fans with three layers of porous ceiling; [d]N/A: not applicable; [e]The exact leak and ignition locations are shown in Fig. 2 and Table 2; [f]S: water spray system (with 25 water spray zones); P: pressure relief panel (set on the sidewall of the subfab); S+P: the combination of a water spray system and a pressure relief panel. The simulation parameters and the exact locations for the water spray system and the pressure relief panel are shown in Table 2 and Fig. 2, respectively.

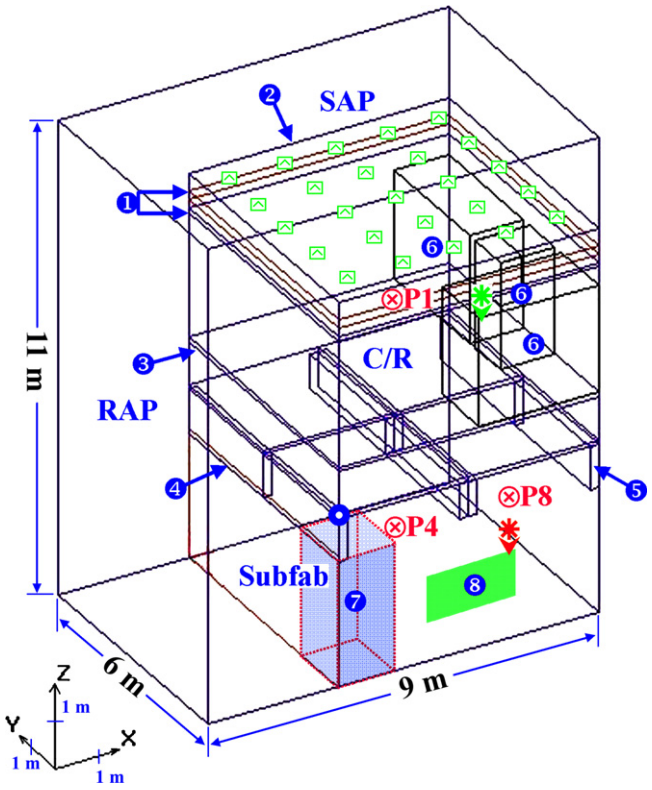

Fig. 2. 3D layout model of a semiconductor plant, where the symbols and numbers denote: (⊗), monitoring points (where P1 is located at the center of the C/R, P4 is located at the center of the subfab, and P8 is located at the corner of the subfab); (⮟), release points (where red/deep grey color represents subfab release and green/light grey color represents C/R release); (✱), ignition points (where red/deep grey color represents subfab ignition and green/light grey color represents C/R ignition); (⭘), origin of the 3D model, where its coordinate equals (0, 0, 0); (▱), airflow modelling fans; (1) filter, where three layers of porous ceiling are employed to simulate the function of the HEPA/ULPA filters; (2) FMU layer, where 25 modelling fans are located to simulate the function of the FMUs (see Table 1); (3) perforated raised-floor, where one layer of porous floor is employed to simulate its function; (4) top of the water spray system (total 25 zones); (5) beam/support; (6) semiconductor machineries; (7) water spray zone No. 1 (blue/grey shaded area, see Table 2 for details); (8) pressure relief panel (green/light grey area, see Table 2 for details).

validating the software were published in the literatures [14–18].

(3) Flow visualization (Flowvis)

This is a post-processing module that can convert the calculation results (approximately 50 kinds of physical variables) into variable-time curves, 2D contour plots, 3D plots, or volume plots in a static/dynamic form as required by the user.

3.2. Model construction and scenario enumeration

In this research, a 3D semiconductor factory model (9 m-long, 6 m-wide and 11 m high) with a FMU SAP design was constructed using the CASD module (see Fig. 2). Three different sizes of machineries were placed above a perforated raised-floor (the "air permeability" or the "degree of porosity" of the simulated floor was set at 0.3). In order to simulate a common semiconductor C/R (airflow rate and type: 0.25–0.3 m s^{-1} ±20%, laminar flow; room temperature: 23 ± 0.2 °C; pressure difference between indoor and outdoor: 14.7–29.4 Pa [9]), dozens of airflow generation types and layouts were proposed and improved accordingly to fulfill the requirements (only three representations are shown in Table 1, Scenarios 1A to 1C).

After the airflow generation types and layouts were chosen, different release scenarios and parameters were designed (see Table 1, Scenarios 2–6). The released gas species employed in this research were hydrogen and propane, while the former is commonly used

Table 2
List of boundary conditions and other parameters used in FLACS simulations

Item	Setting	Contents
Boundary conditions		
X_{LO}, X_{HI}	EULER	–
Y_{LO}, Y_{HI}	EULER	–
Z_{LO}, Z_{HI}	EULER	–

Item	Unit	Value
Parameters for 25 fans (with three layers of porous ceiling)		
Total number	–	25
Type	–	"AIR JET"
Open sides	–	"$-Z$ = $+Z$"
Start time	s	0
Duration	s	50
Area	m^2	0.04
Velocity	m s^{-1}	21
Relative turbulence intensity	–	0.03
Turbulence length scale	m	0.01
Temperature	°C	23
Position	–	At the FMU layer (see Fig. 2)

Item	Unit	Value
Parameters for leaks and ignitions		
Type	–	"JET"
Open sides	–	"$+Z$"
Release start time	s	30
Release duration[a]	s	10
Area	m^2	5.07×10^{-4}
Mass flow[b]	kg s^{-1}	0.2
Relative turbulence intensity	–	0.15
Turbulence length scale	m	0.01
Temperature	°C	23
Ignition start time	s	30

Position		C/R	Subfab
Coordinate (leak points)	m	(4.2, 3.0, 3.0)	(5.6, 2.8, −2.8)
Coordinate (ignition points)	m	(4.0, 2.8, 3.2)	(5.2, 2.8, −2.8)

Item	Unit	Value
Parameters for water spray system		
Total zone number	–	25
Position	–	At the subfab (see Fig. 2(7))
Size of single zone ($x \times y \times z$)[c]	m	$1.2 \times 1.2 \times 3.0$

Scenarios		5A	5C	5B
D_m	μm	700	846	1000
β_{water}	‰	0.24	0.20	0.17
P_w	Pa	2.92×10^5	1.65×10^5	1.00×10^5
U_z	m s^{-1}	1.79	2.14	2.50
Q	m^3 s^{-1}	6.2×10^{-4}	6.15×10^{-4}	6.13×10^{-4}

Item	Unit	Value
Parameters for pressure relief panel		
Total number	–	1
Position	–	At the subfab (see Fig. 2(8))
Size ($x \times z$)	m	2.0×1.0
Panel type	–	Pop-out
Opening pressure difference	Pa	2×10^3
(Po_i, Po_f)	–	(0.0, 1.0)
Weight	kg m^{-2}	10.0
Sub-sizes ($x \times z$)	m	2.0×1.0

[a] It is assumed that the emergency shutoff (EMO) device activated successfully after 10 s of gas leak.

[b] This item is set at 0.4 kg s^{-1} in Scenario 4B.

[c] All 25 water spray zones have equal size.

in a semiconductor manufacturing process and the latter is used for an off-gas cleaning process. Their individual fire and explosion consequences were compared. Different release sites (subfab and C/R) and leak rates (0.2 and 0.4 kg s^{-1}) that may influence the flow pattern, flammable cloud size, and its incident outcomes were studied. Finally, a variety of mitigation measures such as a water spray system with different drop diameters, a pressure relief panel, and the combination effect of the aforementioned measures were also investigated. The corresponding parameters and boundary conditions are listed in Table 2 for further reference. All the simulation results were observed from specific monitoring points (P1, P4, or P8 in Fig. 2) and their corresponding physical variables were plotted as diagrams for comparison.

Usually the finer the grid cells are, the better the fluid field resolution and longer the calculation time will be. In certain circumstances, owing to the round-off error, some finer grids even lead to unstable simulation conditions and incorrect results [7,19]. Since the grid size (or grid numbers) can affect the calculation time, accuracy, and simulation stability, an "independent test of grid size/fluid field" was executed to find out the best suitable grid size and the most real-approximated fluid field performance (flow stability, flow pattern, and the ability of recirculation) before all the simulation scenarios were implemented.

4. Results and discussion

4.1. Independent test of grid size and fluid field

Seven sets of simulation grids were proposed to undertake the grid-independent test (see Table 3). Numerical computations were carried out on a workstation employing two 2.4 GHz Intel Xeon processors. Run times were approximately 2–72 h for different grid shapes/numbers. Grids 1–4, which are "cubic grids" with equal edge lengths, have the same shapes but different sizes. Grids 5–7 belong to the "rectangular grids" with unequal edge lengths; they have neither the same shapes nor the same edge lengths. The 3D layout model (Fig. 2) was divided into different grid numbers according to the corresponding grid features. The overpressure of the air within the C/R (at Monitor P1) was employed as the performance index and its simulation results can be seen in Fig. 3. It shows that the air overpressures of Grids 3 and 4 have almost reached a stable convergent value after 5 s of simulation time while the values of Grids 5–7 are scattered around. By considering the balance among the accuracy, stability, and calculation time, Grid 3 ($45 \times 30 \times 55 = 74{,}250$) was chosen to form the simulation grids (see Fig. 4) for simulating the FMU fluid fields, the hazard consequences, and the results of different mitigation measures.

The "LEAKS" function of FLACS can provide up to and including 50 nozzles or 25 fans to generate airflow. Fig. 5(a) is the simulation result of Scenario 1A with 36 nozzles and one RAP fan (see Table 1). Although the fluid field in the C/R behaved like a laminar flow, the abundant airflow ejected from the 36 nozzles continuously increases the pressure within the semiconductor factory. This phenomenon is just like someone who uses 36 straws at the same time to blow up a balloon, except in Scenario 1A where only the pressure but not the volume increased inside the factory. On the other hand, owing to the limitation of the fan numbers, the fluid field of Scenario 1B is not only unstable but also generates reverse flows at the inter-space between fans (see Fig. 5(b)). In order to correct these drawbacks, three layers of porous ceiling (behaving like filters, 20 cm and 40 cm in space and their porosity degree all

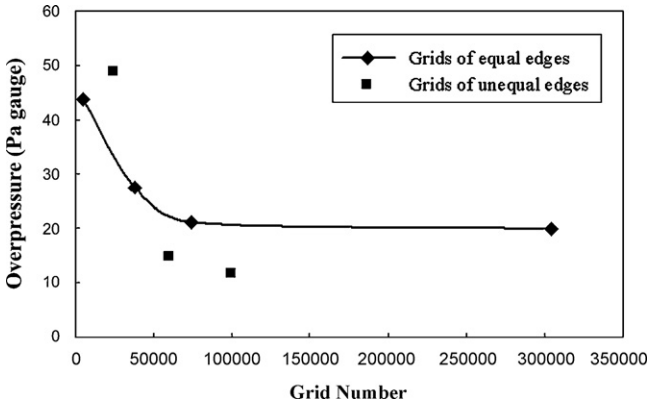

Fig. 3. The influence of different simulation grid shapes/numbers on the air overpressure values under the CFD modeling of a semiconductor factory. The simulation time is 5 s.

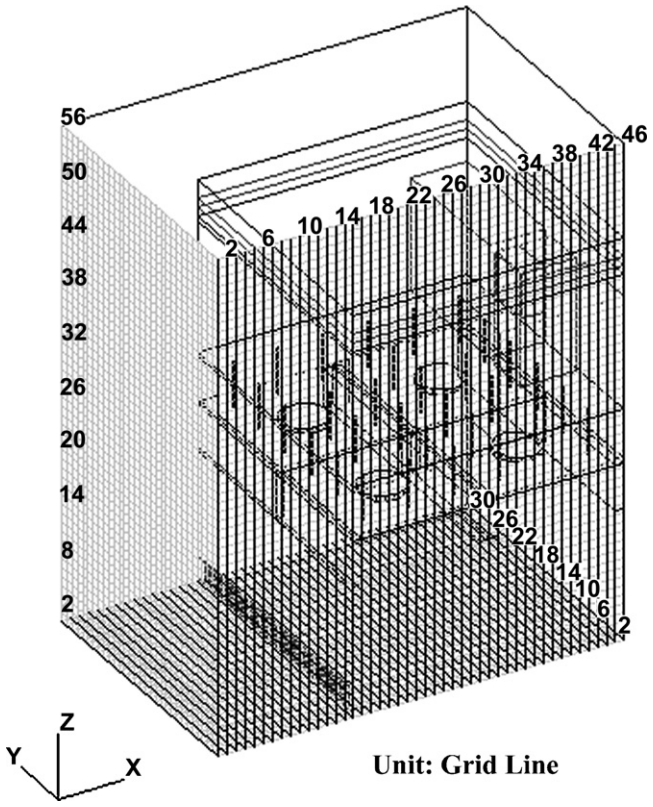

Fig. 4. Final allocation of the simulation grids used for Scenarios 1–6. Each grid equals 0.2 m.

Table 3
Different grid specifications used in grid-independent test

Grid code	Grid 1	Grid 2	Grid 3	Grid 4	Grid 5	Grid 6	Grid 7
Grid category	Equal edges	Equal edges	Equal edges	Equal edges	Unequal edges	Unequal edges	Unequal edges
Total grid number	4,752	38,016	74,250	304,128	24,000	59,400	99,000
Grid number $x \times y \times z$ in (X, Y, Z) axis	$18 \times 12 \times 22$	$36 \times 24 \times 44$	$45 \times 30 \times 55$	$72 \times 48 \times 88$	$30 \times 20 \times 40$	$45 \times 30 \times 44$	$45 \times 40 \times 55$
Unit grid dimension (m) in (X, Y, Z) axis	(0.5, 0.5, 0.5)	(0.25, 0.25, 0.25)	(0.2, 0.2, 0.2)	(0.125, 0.125, 0.125)	(0.3, 0.3, 0.275)	(0.2, 0.2, 0.25)	0.2, 0.15, 0.2)

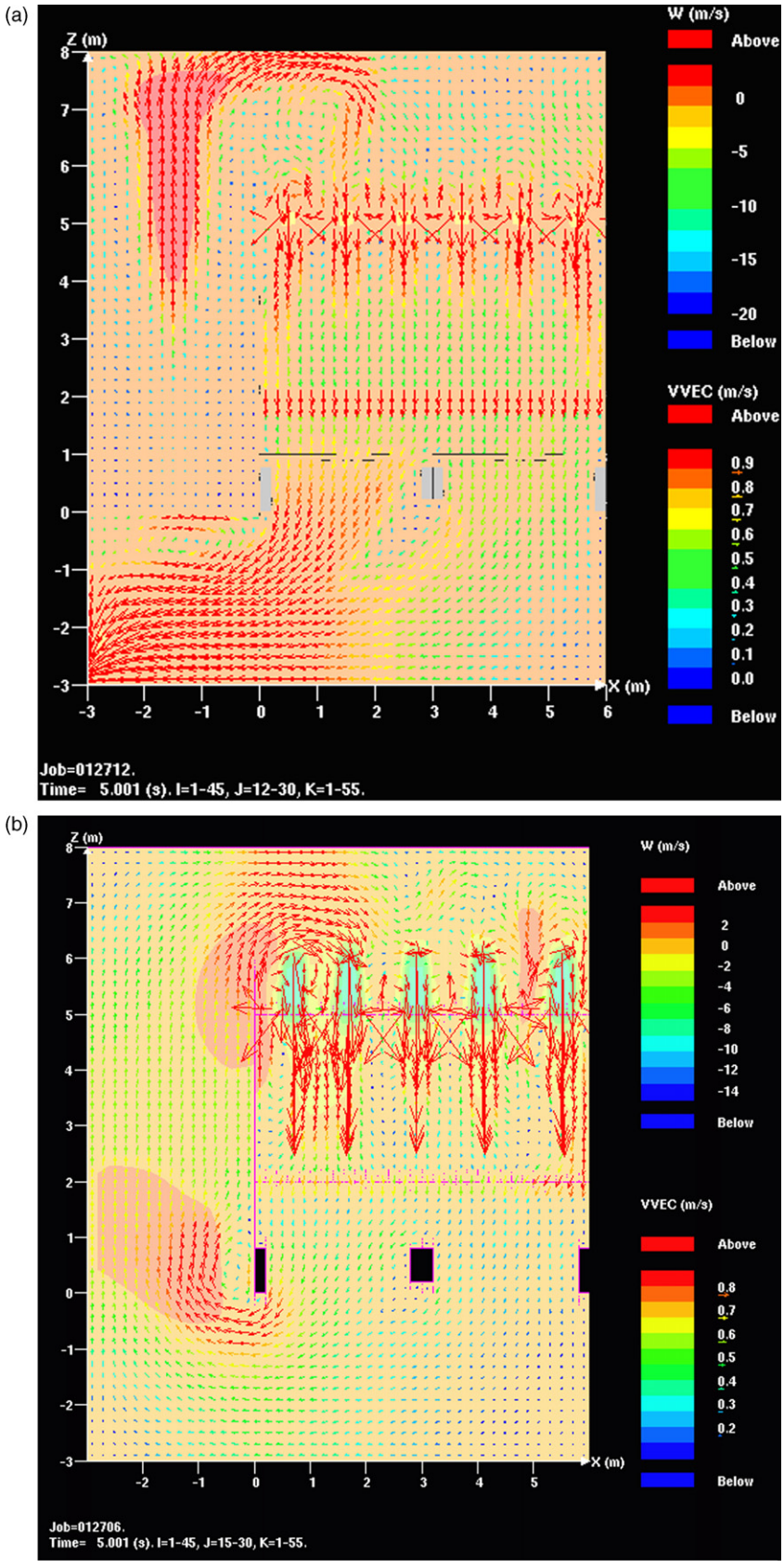

Fig. 5. Simulation results of the velocity fields for different airflow modeling designs: (a) Scenario 1A, (b) Scenario 1B and (c) Scenario 1C. The simulation time is 5 s.

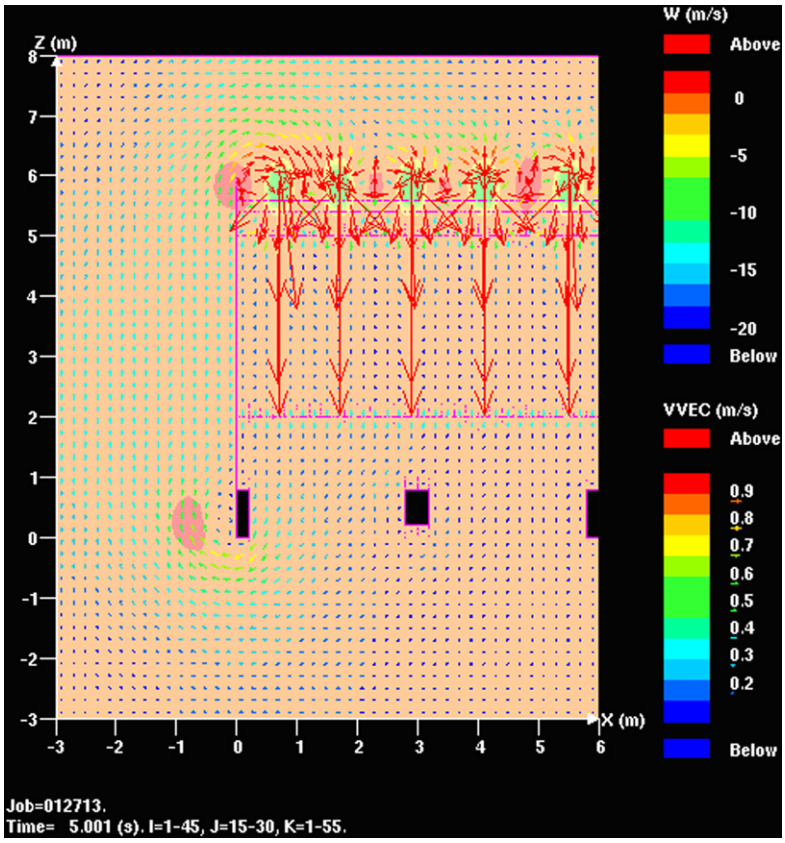

Fig. 5. (*Continued*).

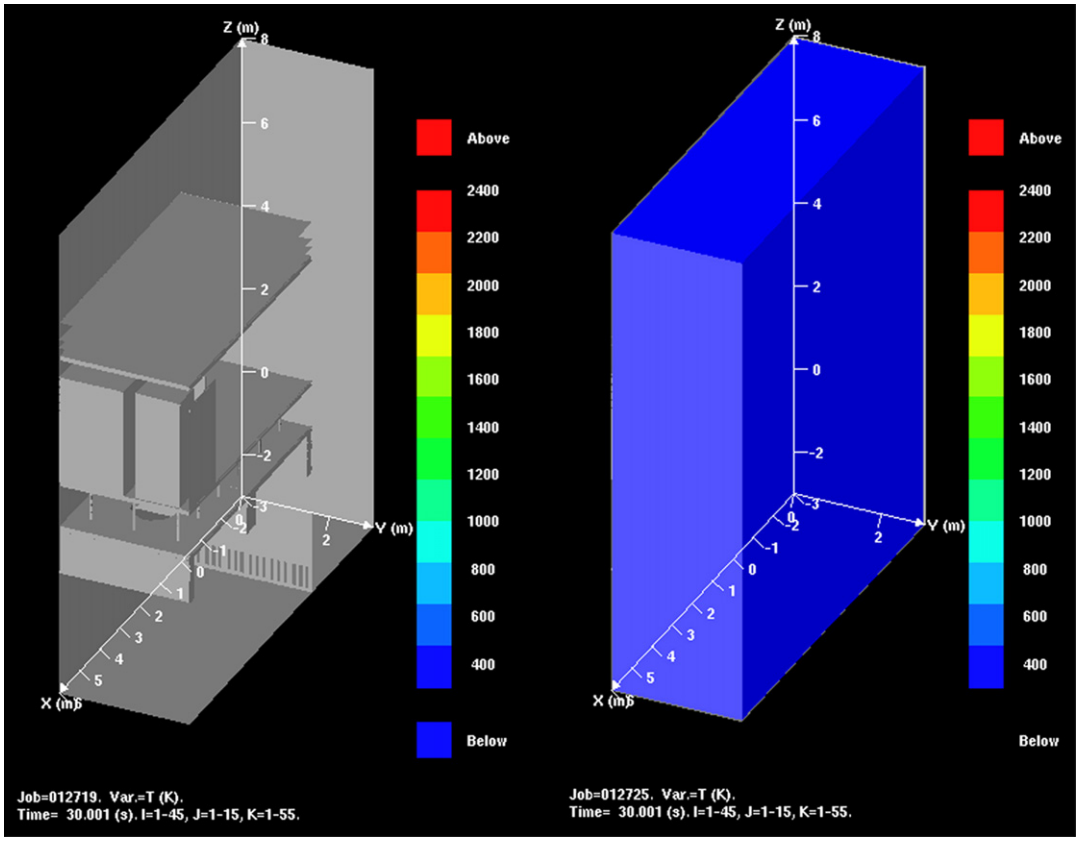

Fig. 6. 3D cross-sectional temperature diagrams of a propane fire and explosion accident without (left, Scenario 2A/3A/4A) and with (right, Scenario 6C) mitigation measures at different time periods: (a) 30.001 s, (b) 30.2 s, (c) 35.0 s, (d) 42.6 s and (e) 49 s.

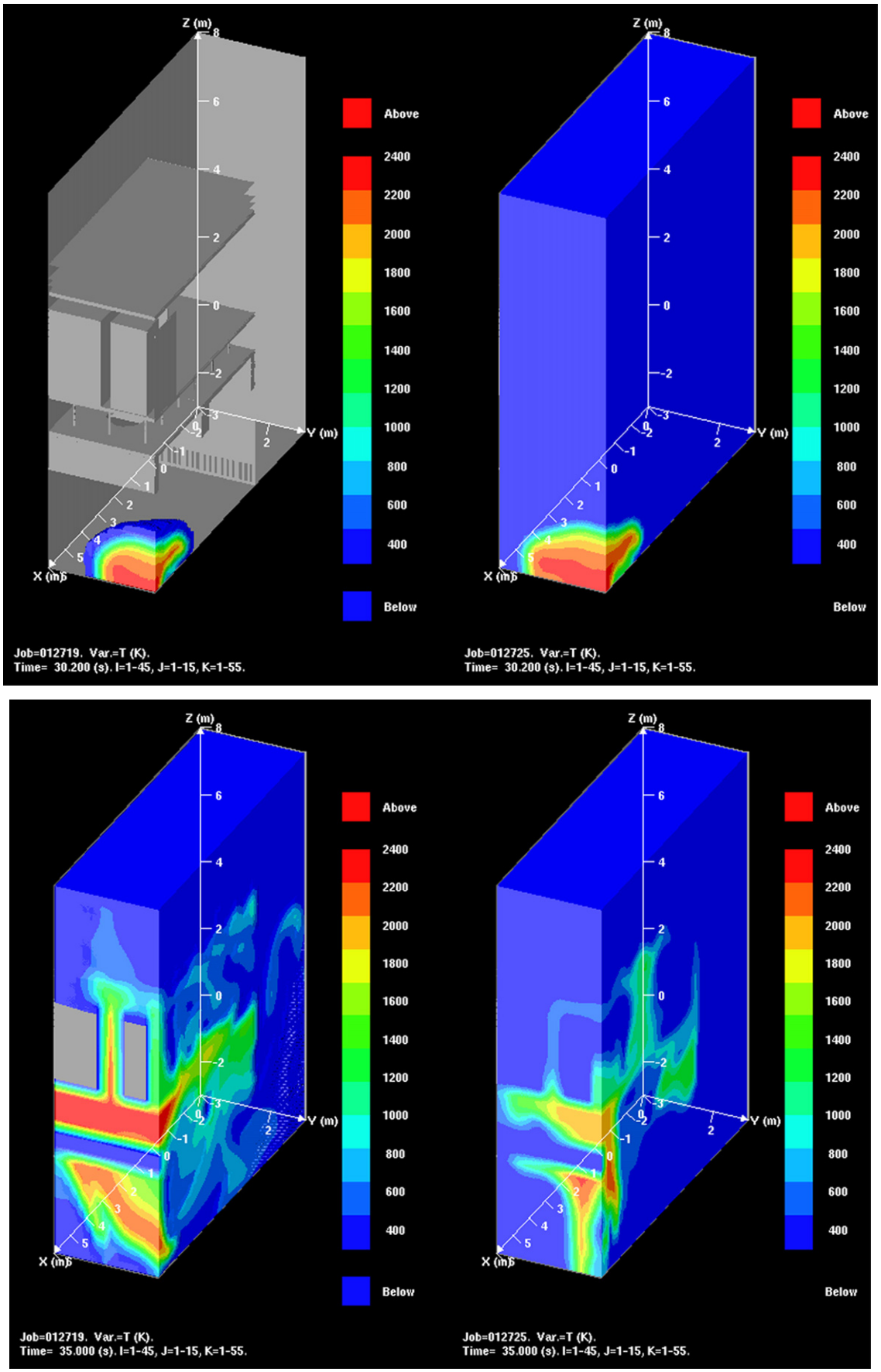

Fig. 6. (*Continued*)

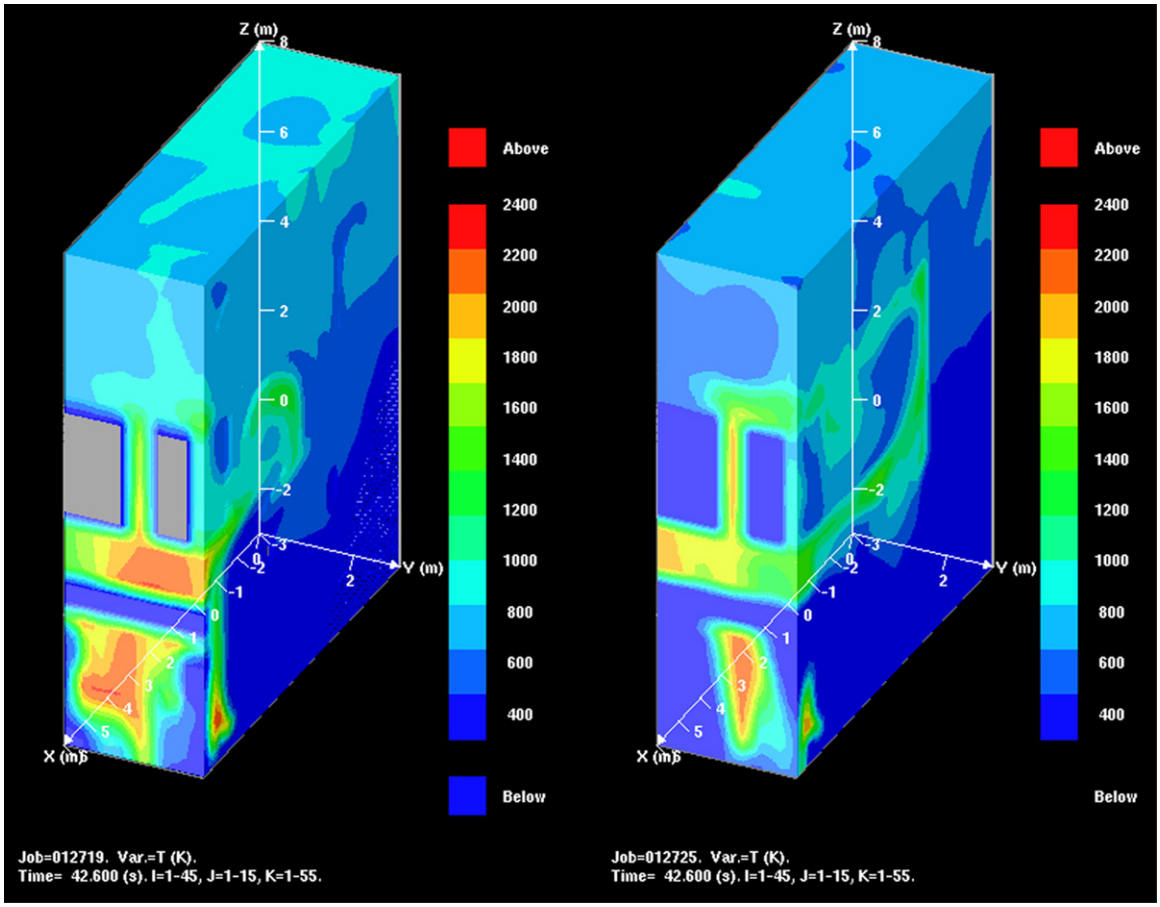

Fig. 6. (*Continued*)

equaling 0.3) were added to provide the flow rectifying effect. The result of Scenario 1C is shown in Fig. 5(c). As can be seen, a laminar, recirculated, and stable fluid field is reached in this design. The longest arrows represent the airflow rates at the FMU layer. As indicated by the shorter arrows, the speed of these airflows decreases to a stable value ($0.25\,m\,s^{-1}$) while the airflows pass through the consecutive layers of porous ceiling.

4.2. Comparison of hazard consequence analyses under different conditions

The left-hand sides of Fig. 6(a)–(e) list the 3D cross-sectional temperature distribution values of Scenarios 2A/3A/4A in different time periods. Within these figures, half of the factory's width (on the *y*-axis) has been cut off on $y = 3$ m to easily observe the inner dynamic behaviors of temperature variation. The ignition start time is set at 30 s after the wind field has stabilized and the flammable gas has just been released. The ignition point is decided by a preliminary gas dispersion test (without ignition). According to the simulation result, one can identify some possible ignition areas where the released gas has been diluted within its flammable/explosive limits around the ignition time. All the related simulation parameters such as starting time, duration, release points, and ignition points can be observed from Table 2 and Fig. 2.

One can see from Fig. 6(a) through (e) that nothing happened in the beginning (30.001 s). However, a deflagration suddenly erupted at 30.2 s near the ignition point (see Fig. 2) with a core temperature of 2400 K. Since the release is directed upward (see Table 2), the ignited flame was driven back into the opposite direction of the airflow and tried to enter the C/R. Five seconds after ignition (35 s), the blaze had penetrated the perforated raised-floor and the C/R was set on fire. The highest temperature region appearing at this time was located between the perforated raised-floor and the airflow guide pits. Owing to the interaction between the released gas and the downward airflow, the blaze swayed unstably in all directions. At 42.6 s, the high temperature air began to circulate back into the SAP and RAP regions. Just before the end of the simulation (49 s), almost over two-thirds of the factory had already been engulfed in a high temperature environment that was larger or equal to 1000 K while a fire was still burning in the subfab. Unlike the temperature field that spread so unevenly, the overpressure field evenly increased (see curve (1) in Fig. 7(a)) from 0 Pa gauge (30 s) to 8.0×10^3 Pa gauge (31 s), 5.4×10^4 Pa gauge (35 s), 9.8×10^4 Pa gauge (42.6 s), and finally reached the highest value of 1.4×10^5 Pa gauge (50 s).

Table 4 summarizes the simulation results from Scenarios 2–6. Scenario 2B represents the fire and explosion consequence of hydrogen released in a subfab. Its peak overpressure (2.40×10^4 Pa gauge) and peak temperature (1802 K) are obviously smaller than those of propane (1.40×10^5 Pa gauge, 2294 K) if all the other conditions remain the same as Scenario 2A. Since propane is heavier than hydrogen, its concentration is not easy to be diluted by airflow and thus leaves a larger gas cloud within the flammable limits at the subfab. This could cause an even more severe fire and explosion consequence than hydrogen. When a propane release happens in a C/R (Scenario 3B), it was found that its hazard consequences (1.06×10^5 Pa gauge, 2242 K) are smaller than those of the subfab (Scenario 2B). It is postulated that the air mixing and exchange efficiency of the C/R (without any dead ends) is better than that

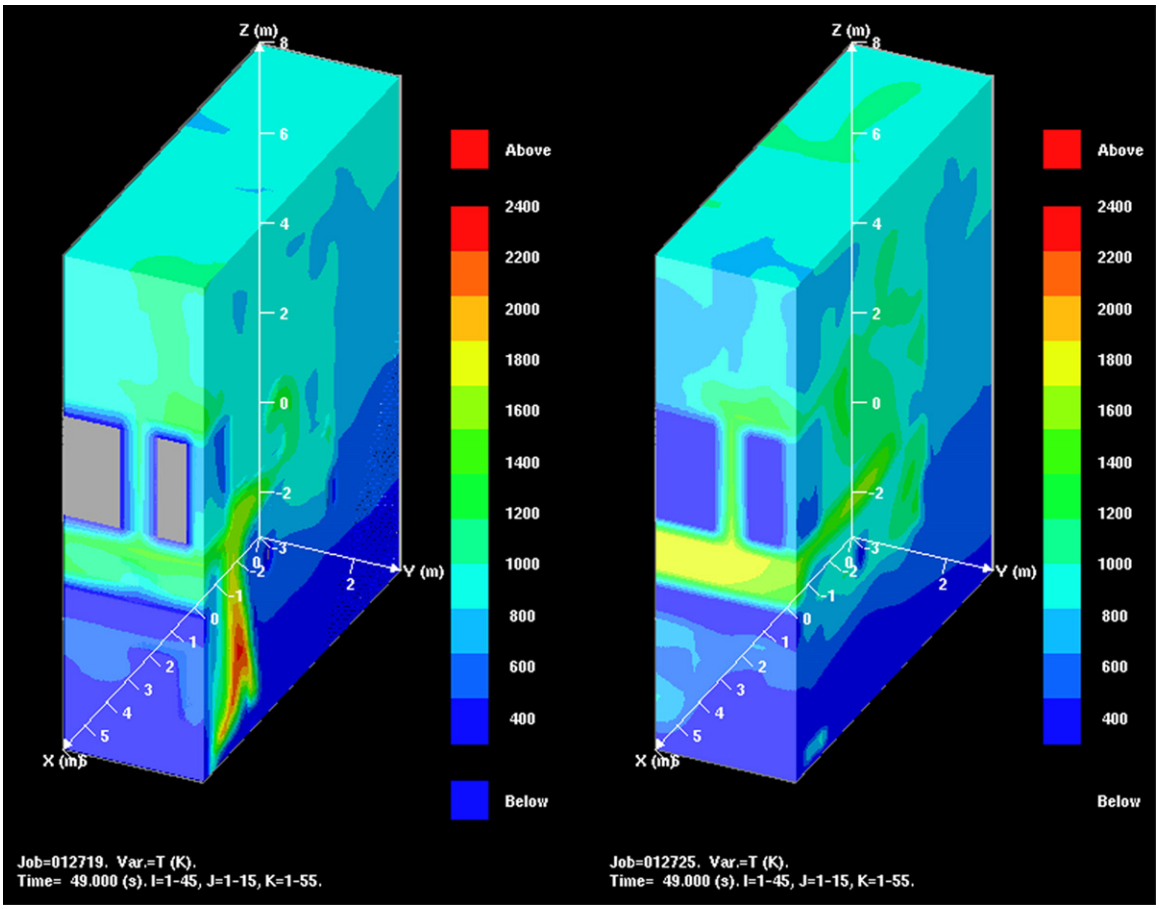

Fig. 6. (*Continued*).

of the subfab (with room corners). Therefore, the flammable gas cloud of the latter is not easy to be diluted by airflow especially near the corners. When the propane leak rate is raised from 0.2 to 0.4 kg s^{-1} (Scenario 4B), its peak overpressure soon increases to 3.00×10^5 Pa gauge that may severely damage the facilities inside the factory. This demonstrates that a greater leakage can produce a larger flammable cloud and thus can cause an even more severe consequence.

4.3. Comparison of different mitigation measures

Figs. 7(a) and 8(b) demonstrate the transient overpressures and temperatures of the simulation results that were recorded by Monitor P8 before and after different mitigation measures were employed (where (1) denotes Scenarios 2A/3A/4A, (2) denotes Scenarios 5C/6A, (3) denotes Scenario 6B, and (4) denotes Scenario 6C). Table 4 lists their corresponding peak values of the above scenarios. It is observed from Fig. 7 or Table 4 that the deflagration temperature can be quickly controlled if the parameters of the water spray system such as water droplets, water pressure, and so on (see Table 2) are properly selected. Scenario 5C shows when 25 water spray zones (see Table 1 and Fig. 2) were deployed at a subfab with the water droplet diameter (D_m) set at 846 μm, the peak temperature of the accident area quickly dropped from 1600 to 800 °C (compare with Scenarios 2A/3A/4A). However, an even more severe consequence may also happen if the D_m value is inappropriately chosen (such as 700 and 1000 μm in Scenarios 5A and 5B). This is because whenever a water droplet is too large or too small under a certain supply pressure, the water droplet will not be broken up by the impulse pressure and will be washed away by the blast or become an obstacle, thus causing a turbulent flow. These small obstacles can accelerate the flame front, therefore causing an earlier rise of pressure and a higher overpressure. These phenomena explain why the overpressure in a deflagration site with only a water spray system can still increase continuously although its temperature has already dropped to a lower level (compare Sce-

Table 4
List of results for different simulation scenarios

Scenario code	2A/3A/4A	2B	3B	4B	5A	5B	5C/6A	6B	6C
Peak overpressure (Pa gauge)	1.40×10^5	2.40×10^4	1.06×10^5	3.00×10^5	1.52×10^5	1.54×10^5	1.46×10^5	2.00×10^4	2.20×10^4
Peak impulse pressure (Pa s)	1.60×10^6	2.54×10^5	1.20×10^6	3.25×10^6	1.72×10^6	1.73×10^6	1.70×10^6	2.00×10^4	2.10×10^4
Peak temperature (K)	2294[a]; 1600[b]	1802[a]	2242[a]	2353[a]	1842[b]	1852[b]	800[b]	1613[b]	650[b]

[a] Measured at monitoring point P4.
[b] Measured at monitoring point P8.

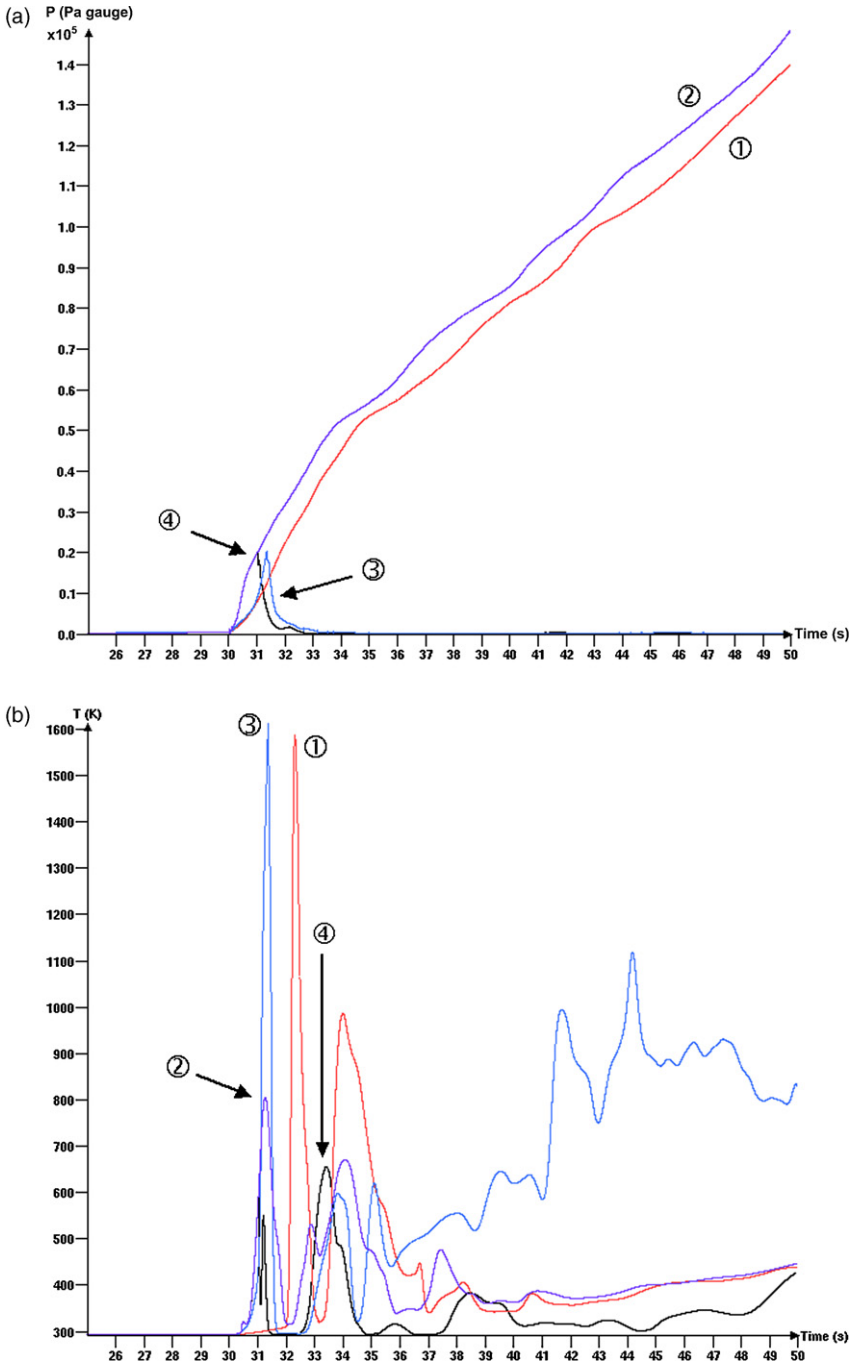

Fig. 7. Overpressure and temperature curves of a propane fire and explosion accident recorded by monitor P8: (a) overpressure–time curves, (b) temperature–time curves. Where the numbers denote: (1) Scenario 2A/3A/4A, without any mitigation measures; (2) Scenario 5C/6A, with a water spray system (D_m = 846 mm) only; (3) Scenario 6B, with a pressure relief panel only; (4) Scenario 6C, with a water spray system and a pressure relief panel.

narios 5C/6A with Scenarios 2A/3A/4A in Table 4 or observe curves (1) and (2) in Fig. 7).

By comparing Scenarios 2A/3A/4A with Scenario 6B in Table 4, it can be seen that the peak overpressure dropped from 1.40×10^5 to 2.00×10^4 Pa gauge when the pressure relief panel (see Tables 1 and 2 and Fig. 2) was activated. In this case, the peak temperature of the accident area still remains at a high value of about 1600 K, which can cause serious damage to both operators and equipment. The aforementioned situation can also be observed by comparing the overpressure and temperature values of curves (1) and (3) in Fig. 7. Moreover, one can find out from Fig. 7(b) that the appearance time and value of the maximum temperature of curve (3) are even earlier and higher than those of curve (1). It is speculated that abruptly opening the relief panel could cause a strong current to flow out of the factory. This turbulent current could initiate a positive flame accelerating effect, thus causing the deflagration reaction to take place earlier and stronger. However, the overpressure buildup decreases very quickly because the relief panel has already been opened. Only the temperature effect still exists since the C/R itself is not totally empty and the continuously released propane can sustain the reaction. After the initial peak of curve (3) appears in Fig. 7(b), the temperature curve goes

up and down for several times, and then gradually climbs up to an average value of 900 K. The former phenomenon is due to the swaying of the flame, which can also be seen from curve (1) or from Fig. 6(c)–(e); the latter phenomenon is probably caused by a temperature buildup in the SAP and RAP, which later recirculates into the subfab zone. It looks like this continuously ascending temperature phenomenon has a tendency to evolve from deflagration to detonation. However, this transition effect cannot happen since the release has already been terminated at 40 s (see Table 2) and, as a result, the overpressure cannot build up under such circumstance. Should the material be a highly reactive chemical and be continuously released in a very quick and large manner while flowing through a highly congested and mostly confined region, such DDT (deflagration to detonation) phenomena might happen after the relief panel is activated [20].

When the water spray and the pressure relief panel were activated simultaneously, the peak overpressure and the peak temperature both dropped to 2.20×10^4 Pa gauge and 650 K, respectively (see Scenario 6C in Table 4). Although the overpressure can still cause a certain amount of damage, the combination result of both measures can really mitigate most of the serious threats. Its transient phenomena can be observed either from Fig. 7 or from Fig. 6. By observing curve (4) in Fig. 7(a), one can see that the highest peak overpressure happens at 31 s. After that period, the overpressure drops to zero again. From the right-hand sides of Fig. 6(a)–(e), one can also find out their temperature developing situations are similar to those of Scenarios 2A/3A/4A that have been discussed before in Section 4.2 (compare the right-hand sides with the left-hand sides of Fig. 6(a)–(e)). These similar temperature-developing trends can also be found via comparing curve (4) with curve (1) in Fig. 7(b), except curve (4) shows an earlier appearance for the corresponding temperature peaks and much lower temperature values. Again, this is caused by the obstacle and cooling effect of the water mist droplets. Another valuable observation is that after the gas release has stopped, the subfab fire of Scenario 6C can be quickly put out by two simultaneous mitigation measures, but Scenarios 2A/3A/4A cannot (see Fig. 6(e)). However, it seems that the C/R damage of Scenario 6C is more serious than that of Scenarios 2A/3A/4A. Such phenomenon cannot be observed in Fig. 7 since it only reveals a local view and not a global view.

5. Conclusions

Owing to its confined manufacturing environment, special airflow pattern, and lack of proper tools, the semiconductor industry still has not currently developed a proper consequence analysis procedure that can facilitate a loss prevention design for fire and explosion accidents. By employing FLACS software, which is commonly used in petrochemical fire and explosion simulations, this research has proposed a deliberatively designed 3D model that can vividly simulate the fan-filter function and reconstruct the air recirculation flow pattern within a real semiconductor factory.

After the air recirculation behavior had been properly constructed, different hazard scenarios were proposed and simulated and various mitigation measures were provided to evaluate their efficiency. It was found that when a $0.2\,kg\,s^{-1}$ propane leak happened and ignited in a subfab area without any mitigation measures, the fire and explosion results within 20 s (peak overpressure = 1.40×10^5 Pa gauge; peak temperature = 1600–2294 K, at different monitoring points) could cause permanent damage to the equipment while personnel within the area would never have enough time to escape. With a proper water spray system installed (D_m = 846 μm), the temperature can be decreased to a certain limit while the overpressure still remains very high. On the other hand, the overpressure can drop immediately while its temperature remains very high if the pressure relief panel is activated. The temperature and overpressure can both be reduced efficiently (peak overpressure = 2.20×10^4 Pa gauge; peak temperature = 650 K) only when different mitigation measures are integrated and implemented at the same time. Through the 3D dynamic demonstrations of the overpressure and temperature field of different hazard scenarios and their countermeasures, this simulation method can provide the related personnel a quick and easy way to gain insights into the mitigation designs for all kinds of fire and explosion hazards that could happen within a confined air recirculation environment.

Acknowledgements

The authors are grateful to the GexCon AS, Norway for providing the FLACS software and to the National Science Council of Taiwan for its partial financial aid of this study under the project number NSC 94-2211-E-224-007.

References

[1] J.R. Chen, Characteristics of fire and explosion in semiconductor fabrication processes, Process Safe. Prog. 21 (2002) 19–25.
[2] D.D. Herrmann, Improved vapor cloud explosion predictions by combining CFD modeling with the Baker–Strehlow method, in: Proceeding of International Conference and Workshop on Modeling the Consequence of Accidental Releases of Hazardous Materials, San Francisco, USA, 1999, pp. 479–494.
[3] O.R. Hansen, O. Talberg, J.R. Bakke, CFD-based methodology for quantitative gas explosion risk assessment in congested process areas: examples and validation status, in: Proceeding of International Conference and Workshop on Modeling the Consequence of Accidental Releases of Hazardous Materials, San Francisco, USA, 1999, pp. 457–477.
[4] S. Høiset, B.H. Hjertager, T. Solberg, K.A. Malo, Flixborough revisited—an explosion simulation approach, J. Hazard. Mater. 77 (2000) 1–9.
[5] H.S. Ledin, C.J. Lea, A review of the state-of-the-art in gas explosion modelling, Fire and Explosion Group, UK (2002) HSL/2002/02 http://www.hse.gov.uk/research/hsl_pdf/2002/hsl02-02.pdf.
[6] C.E. Fothergill, S. Chynoweth, P. Roberts, A. Packwood, Evaluation of a CFD porous model for calculating ventilation in, J. Loss Prev. Proc. Ind. 16 (2003) 341–347.
[7] M. Cheng, G.R. Liu, K.Y. Lam, W.J. Cai, E.L. Lee, Approaches for improving airflow uniformity in unidirectional flow cleanrooms, Build. Environ. 34 (1999) 275–284.
[8] W.J. Lee, The outlook of cleanroom for deep submicron semiconductor process, Electron. Monthly 2 (1996) 89–98.
[9] W. Whyte, Cleanroom Design, 2nd ed., John Wiley & Sons, Inc., 2000.
[10] S. Dharmavaram, S.R. Hanna, O.R. Hansen, Consequence analysis—using a CFD-model for industrial sites, Process Safe. Prog. 24 (2005) 316–327.
[11] A.J. Majda, Compressible Fluid Flow and Systems of Conservation Laws in Several Space Variables, Springer, 1984, ISBN 0387960376.
[12] R.S. Brodkey, The Phenomena of Fluid Motions, Brodkey Publishing, 2004, ISBN 0972663576.
[13] B.H. Hjertager, Computer simulation of turbulent reactive gas dynamics, J. Model. Iden. Control 5 (1985) 211–236.
[14] B.H. Hjertager, M. Bjørkhaug, K. Fuhre, Explosion propagation of non-homogeneous methane-air clouds inside an obstructed 50 m3 vented vessel, J. Hazard. Mater. 19 (1988) 139–153.
[15] B.H. Hjertager, K. Fuhre, M. Bjorkhaug, Gas explosion experiments in 1:33 and 1:5 scale offshore separator and compressor modules using stoichiometric homogeneous fuel/air clouds, J. Loss Prev. Proc. Ind. 1 (1988) 197–205.
[16] C. Catlin, C.A.J. Gregory, D.M. Johnson, D.G. Walker, Explosion mitigation in offshore modules by general area deluge, Trans. I. Chem. E. 71 (1993), Part B 12.
[17] O.R. Hansen, I. Storvik, K. van Wingerden, Validation of CFD-models for gas explosions, where FLACS is used as example: model description and experiences and recommendations for model evaluation, in: Proceedings European Meeting on Chemical Industry and Environment III, Krakow, Poland, 1999, pp. 365–382.
[18] S.R. Hanna, O.R. Hansen, S. Dharmavaram, FLACS air quality CFD model performance evaluation with Kit Fox, MUST, Prairie Grass, and EMU observations, J. Atmos. Environ. 38 (2004) 4675–4687.
[19] S. Nam, Numerical simulation of smoke movement in cleanroom environments, Fire Safe. J. 34 (2000) 169–189.
[20] S.P. Medvedev, S.V. Khomik, H. Olivier, Experimental measurements of explosions with active/passive additives, Institute of Chemical Physics, RAS, Moscow (2004), Report D9, Contract EVG1-CT-2001-00042, WP1.2 – Partner 2 http://batchelor.uc3m.es/expro/D9_SWL.pdf.